JOM, Vol. 72, No. 11, 2020
https://doi.org/10.1007/s11837-020-04377-0

Phase Stability of Ni/Ni_3Al Multilayers Under Thermal Annealing and Irradiation

CHENG SUN ,[1,3,4] STUART A. MALOY,[2] KEVIN BALDWIN,[2] YONGQIANG WANG,[2] and JAMES A. VALDEZ[2]

1.—Idaho National Laboratory, Idaho Falls, ID 83415, USA. 2.—Los Alamos National Laboratory, Los Alamos, NM 87545, USA. 3.—e-mail: cheng.sun@inl.gov. 4.—e-mail: chengsun2008@gmail.com

Nickel-based superalloys with $L1_2$-ordered Ni_3Al precipitates exhibit excellent high-temperature mechanical properties and corrosion resistance. Here we studied the phase stability of a Ni/Ni_3Al multilayer under high-temperature thermal annealing and Ni ion irradiation. Ni/Ni_3Al multilayers with order–disorder interfaces were fabricated by magnetron sputtering at 773 K. Thermally induced interdiffusion and precipitation occurred under thermal annealing at 1073 K for 1 h. Ni ion irradiation at 773 K to a dose of 2×10^{16}/cm^2 led to chemical intermixing across the Ni/Ni_3Al interface, although the Ni_3Al layer remained ordered. The results of this study provide insight into the understanding of disorder, recovery, and dissolution processes occurring in ordered intermetallic compounds in extreme environments.

INTRODUCTION

Understanding physical and chemical processes in extreme conditions is imperative to the discovery and design of materials for applications involving stringent operating conditions. Intermetallic compounds with excellent high-temperature strength, creep, and corrosion resistance are promising for application in advanced nuclear reactors.[1–4] Ni-based alloy 617 has been considered as a structural material for very-high-temperature reactors (VHTRs) for components operating at temperatures up to 1223 K.[5] The formation of intermetallic compounds, such as nickel aluminides, results in precipitation strengthening and creep resistance. γ' and γ'' are two typical intermetallic compounds in Ni-based alloys. γ' is identified as $Ni_3(Al,Ti)$ with $L1_2$-ordered face-centered cubic (fcc) structure, whereas γ'' denotes the ordered Ni_3Nb with DO_{22} body-centered tetragonal (bct) structure. In Ni-based alloys, the cohesive interface between the Ni-based matrix and the intermetallic compounds could give rise to a good combination of mechanical properties and oxidation resistance. The formation of a γ/γ' lamella structure results in an increase in the compressive strength of Ni-12.6Al-20Ir-5Nb refractory superalloys that depends on the volume fraction and orientation of the lamellar structure.[6] Fractography of Ni/Ni_3Al multilayers reveals ductile failure in both Ni and Ni_3Al layers without interface delamination.[7] The ultrafine-grained Ni-based fcc structure with finely dispersed γ' Ni_3Al phase accelerates the formation of continuous alumina layers, thereby improving the oxidation performance of γ/γ' composite in air at 1273 K for 20 h.[8]

In the core of a nuclear reactor, materials must withstand an exceptionally extreme environment, including high temperatures and intense irradiation fluxes.[9] Study of the stability of γ/γ' interfaces at high temperatures and under irradiation is therefore vital to their engineering applications in the nuclear industry. During thermal annealing at temperatures ranging from 1073 K to 1323 K for 1000 h, the γ' particles coarsen with a kinetics that is consistent with a linear relationship for Ostwald ripening.[10] The morphology of the γ' phases in γ'/γ interfaces evolves from sphere to rod-like, and foliated γ' phases formed eventually with increasing thermal exposure time.[11] Long-term exposure of the γ'' intermetallic compound in Ni-based alloys at 923–1023 K led to a phase

(Received June 16, 2020; accepted September 9, 2020; published online September 24, 2020)

transformation to δ phases, resulting in a considerable loss of ductility.[12] The irradiation environment in nuclear power plants could cause intermetallic compounds to suffer various forms of degradation in operation, such as phase transformation, swelling, embrittlement, etc.[13–16] It has been reported in literature that the ordered γ' and γ'' precipitates are susceptible to irradiation damage and readily became disordered, especially at relatively low temperatures. Our previous work on Ni-based superalloy Rene N4 showed that such disordering of cuboidal γ' precipitates occurred at 0.3 dpa under Kr ion irradiation at room temperature.[17] Proton irradiation of Inconel 718 alloy showed that the order–disorder transformation of γ' and γ'' precipitates started at 0.1 dpa and completed at 0.7 dpa at room temperature.[18] The radiation-induced order–disorder transformation of γ' and γ'' precipitates is attributed to the ballistic effect of ion bombardment, which disrupts the structural ordering of the precipitates. Some types of intermetallic compound are susceptible to amorphization under irradiation. A molecular dynamic study concluded that such radiation-induced amorphization of ordered intermetallic compounds involves a chemical disorder process followed by the stabilization and accumulation of point defects.[19]

In the work described herein, we fabricated Ni/Ni_3Al multilayers using magnetron sputtering and studied the stability of the $L1_2$ ordered Ni_3Al phase under thermal annealing and irradiation. The order–disorder transition, recovery, and dissolution of γ' Ni_3Al precipitates under thermal annealing and irradiation are discussed. The results of this research provide insight into the degradation mechanism of order–disorder interfaces in extreme environments.

EXPERIMENTAL PROCEDURES

Magnetron sputtering was used to synthesize a Ni/Ni_3Al multilayer film on an MgO substrate at 773 K under vacuum at pressure of 0.399 kPa. The base pressure of the system was 1×10^{-8} torr. Ni_3Al layers were deposited by cosputtering from Al and Ni targets. The direct-current (DC) power used on the Al and Ni targets was varied to obtain the required stoichiometry of Ni_3Al. The total deposition duration was around 20 min. Transmission electron microscopy (TEM) characterization was performed on an image-corrected FEI Titan operated in TEM mode at 300 keV and equipped with energy-dispersive x-ray spectroscopy (EDS). Cross-sectional TEM specimens were prepared by mechanical polishing followed by subsequent low-energy ion milling in a Precision Ion Polishing System (PIPS). To study their thermal stability, the Ni/Ni_3Al multilayer films were annealed at 1073 K for 1 h with gettered Ar flowing through the tube and cooled down to room temperature at a controlled rate of 5 K/min. Grazing-incidence x-ray diffraction (GIXRD) analysis was performed at angles of incidence of 0.5°, 0.75°, and 1° on both as-deposited and as-annealed multilayers to identify the phase components within the films. Ni ion irradiation experiments were performed at an energy of 10 MeV at 773 K to a dose of 2×10^{16} Ni^{++}/cm^2 with a flux of 0.74×10^{13} Ni^{++}/cm^2 s. The stopping and range of ions in matter (SRIM) code was used to predict the profiles of displacement damage and Ni ion concentration in the specimen. The Kinchin–Pease method was used in the calculation with an average displacement energy of 40 eV for Ni and 28 eV for Al.

RESULTS AND DISCUSSION

As-Deposited Multilayer

A Ni/Ni_3Al multilayer structure with various layer thicknesses was designed, as shown in Fig. 1a. A total of seven layers were designed with layer thickness ranging from 5 to 100 nm. To create $L1_2$-ordered Ni_3Al intermetallic compound in the multilayer, magnetron sputtering was performed at 773 K on MgO substrates. Figure 1b shows a cross-sectional TEM micrograph of the as-deposited Ni/Ni_3Al multilayer. Instead of the designed seven layers of Ni and Ni_3Al, only three distinct layers formed on the MgO substrate. The selected-area diffraction (SAD) pattern of the area in Fig. 1b taken along the [001] zone axis is shown in Fig. 1c, showing diffraction spots originating from both the MgO substrate and Ni/Ni_3Al film. MgO(220) and Ni(220) reflections are marked in the SAD pattern. The superlattice reflections from the ordered Ni_3Al(110) and Ni_3Al(220) are also labeled in the SAD pattern. Both Ni and ordered Ni_3Al phase exhibit fcc structure, with a modest lattice mismatch. The chemical distribution across the Ni/Ni_3Al multilayer on theMgO substrate was characterized by EDS line scanning. Figure 1d shows three layers distinguished by chemistry in the as-deposited multilayer, i.e., Ni, Ni_3Al, and Ni-enriched Ni–Al. The thickness of the deposited Ni layer followed the original design, while the deposited Ni_3Al layer was a combination of the designed Ni_3Al and Ni layers with thicknesses of 50 nm and 100 nm. The top Ni-enriched Ni–Al layer was a mixture of Ni and Ni_3Al layer with thicknesses of 5 nm and 50 nm. The TEM micrograph suggests that chemical interdiffusion occurred between Ni and Ni_3Al layers during magnetron sputtering at 775 K, which caused the disappearance of the interfaces when the layer thickness was less than 50 nm. Figure 2 shows high-resolution TEM (HRTEM) micrographs of the MgO/Ni and Ni/Ni_3Al interfaces at the [001] zone axis and the corresponding fast Fourier transform (FFT) patterns of each layer. The finding of Ni(200)//MgO(200) and Ni_3Al(200)//Ni(200) implies a cohesive configuration of the interfaces, in good agreement with the results seen in the SAD pattern in Fig. 1c.

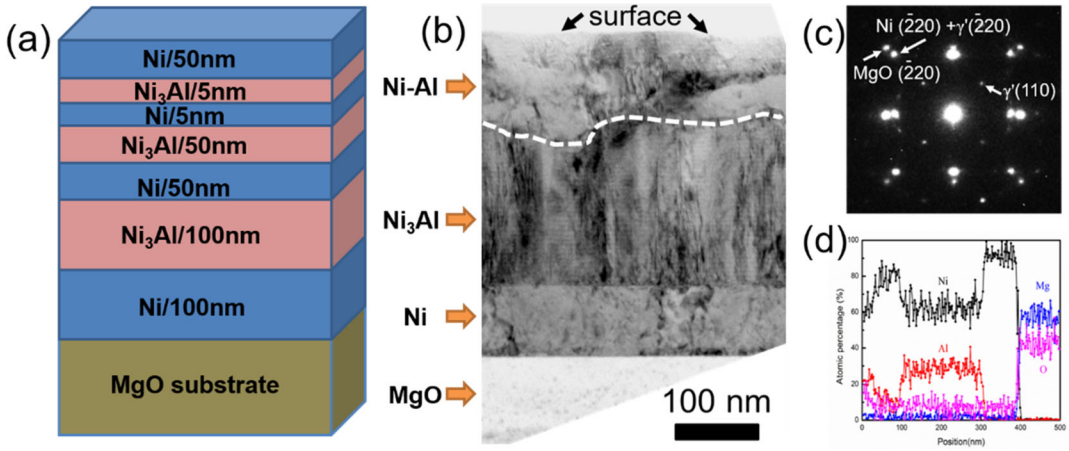

Fig. 1. (a) Schematic of designed Ni/Ni_3Al multilayer structure with layer thickness ranging from 5 to 100 nm. (b) Bright-field TEM micrograph of Ni/Ni_3Al multilayer fabricated by magnetron sputtering at 773 K. (c) SAD pattern showing diffraction spots originating from the ordered Ni_3Al layer, Ni layer, and MgO substrate. (d) EDS line scan across the Ni/Ni_3Al multilayer, showing the distribution of Ni and Al elements.

Fabrication of Ni/Ni_3Al multilayers by magnetron sputtering has been reported in literature, and the multilayer microstructure varies with the sputtering parameters. The substrate temperature and layer thickness are two important tuning parameters that detremine the formation of $L1_2$-ordered Ni_3Al phase in the Ni/Ni_3Al multilayer. The Ni/Ni_3Al multilayer fabricated by magnetron sputtering at room temperature showed a γ Ni–Al solid-solution phase without evidence of ordered Ni_3Al phase, while the ordering transformation from Ni–Al phase to $L1_2$-ordered Ni_3Al takes place after post-sputtering thermal annealing at 773 K and 973 K.[20] At higher deposition temperatures ($\sim$ 723 K), Ll_2-ordered Ni_3Al phase formed in the Ni/Ni_3Al multilayers without post-sputtering heat treatment.[21] Similar to literature reports, $L1_2$-structured Ni_3Al phase was obtained in the Ni/Ni_3Al multilayer by magnetron sputtering at high temperature (773 K) in the current study. Compared with sputtering at room temperature, the lower solidification rate during sputtering at 773 K allows Ni and Al atoms to order chemically and form antiphase domains.[22] It was also observed in the current study that the Ni/Ni_3Al interface became unstable due to chemical interdiffusion for layer thickness less than 50 nm. From a thermodynamic point of view, the Ni/Ni_3Al interface is in a highly nonequilibrium state during sputtering at 773 K. Chemical diffusion along grain boundaries in Ni_3Al could be several orders of magnitude faster than the bulk diffusion process. With decreasing layer thickness, more Ni/Ni_3Al interfaces and columnar boundaries form in the multilayer, resulting in an enhancement of chemical diffusion during sputtering.

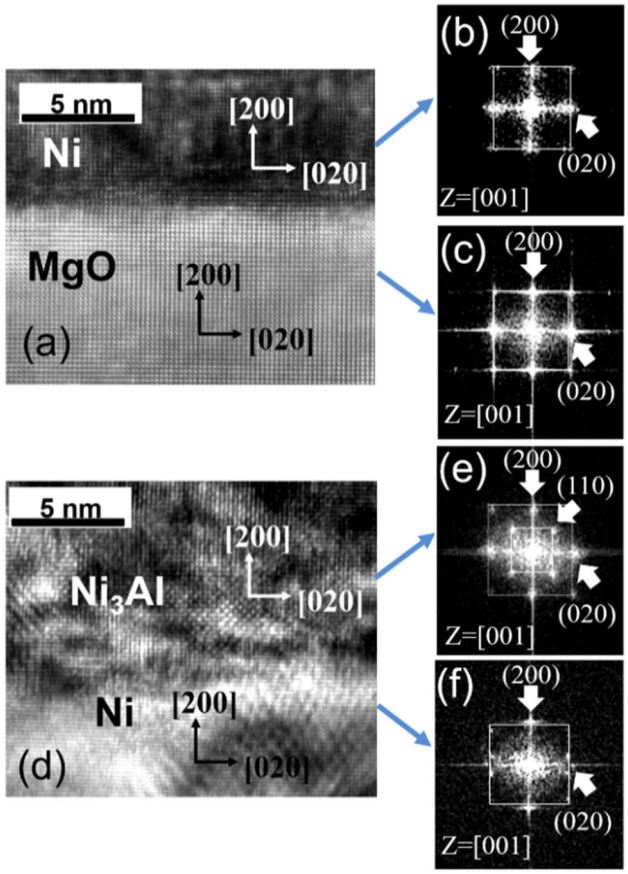

Fig. 2. HRTEM micrographs of interfaces within the Ni/Ni_3Al multilayer: (a) HRTEM micrograph of Ni/MgO interface, showing Ni(200)//MgO(200); (b, c) FFT patterns of Ni layer and MgO substrate. (d) HRTEM micrograph of Ni/Ni_3Al interface, showing Ni(200)//Ni_3Al(200). (e, f) FFT patterns of the Ni and Ni_3Al layer. The Ni_3Al exhibits $L1_2$-ordered structure.

Thermal Stability

The thermal stability of the Ni/Ni_3Al multilayer structure was studied with isothermal annealing experiments. Cross-sectional TEM micrographs of the as-annealed specimens are shown in Fig. 3. In Fig. 3a, the interface of Ni/Ni_3Al becomes discrete with precipitates forming on the interface. Monte

Carlo simulation indicates that the Ni/Ni_3Al interface enhances the vacancy diffusion along the interface and thus promotes the precipitation of the γ' particles on the interface at 1073 K.[23] Figure 3b shows the SAD pattern of the area in Fig. 3a with [110] zone axis. The superlattice reflections are still present in the SAD pattern, suggesting that the $L1_2$-ordered Ni_3Al phase is still present in the as-annealed specimen. Figure 3c shows a weak-beam dark-field (WBDF) TEM micrograph with γ' Ni_3Al diffraction vector of $\mathbf{g} = [111]$. In contrast to the layered structure in the as-deposited multilayer, a high density of γ' Ni_3Al spherical particles was observed within the as-annealed multilayer. The γ' Ni_3Al particles are shown in bright contrast in the WBDF TEM micrograph, as seen in Fig. 3c. The magnified micrograph in Fig. 3d reveals that the average diameter of the γ' phase particles was $\sim$ 5 nm.

GIXRD experiments were performed to characterize the distribution of the $L1_2$-ordered Ni_3Al phase across the Ni/Ni_3Al multilayer. Figure 4a shows the GIXRD diffraction patterns of the as-deposited Ni/Ni_3Al multilayer at angles of incidence of 0.5°, 0.75°, and 1°. The diffraction peaks of Ni/Ni_3Al (110), (111), (200), and (220) were indexed. As the angle of incidence was increased, the peak intensity of the superlattice increased and the intensity of the superlattice diffraction (110) peaks emerged only when the angle of incidence reached 0.75°, suggesting that the concentration of $L1_2$-ordered Ni_3Al phase increased with the x-ray penetration depth. In the as-annealed specimen, the (210) diffraction peak appeared and the intensities of the three major diffraction peaks (111), (200), and (220) did not change dramatically with the x-ray angle of incidence, implying a relatively uniform distribution of $L1_2$-ordered Ni_3Al phase within the multilayer. These GIXRD results agree well with the TEM characterization. The diffraction peak labelled with a star could result from an oxide phase on the surface caused by the thermal annealing. Li et al.[24] reported the formation of Al_2O_3 phase in Ni_3Al film under in situ thermal annealing at 973 K in a TEM.

Irradiation Damage

The irradiation response of Ni/Ni_3Al multilayer was studied using self-ion irradiation at 773 K. The SRIM simulation results shown in Fig. 5a predict that the average displacement damage within the film was $\sim$ 3.5 dpa. A peak displacement damage occurred in the MgO substrate at a depth of $\sim$ 3.5 μm, and the peak concentration of the injected Ni ions decreased in the MgO substrate when moving towards the deposited multilayer, with negligible Ni ions retained within the multilayer. The controlled heat treatment (CHT) represented the unirradiated region of the specimen loaded in the ion accelerator for irradiation, as shown in the experiment

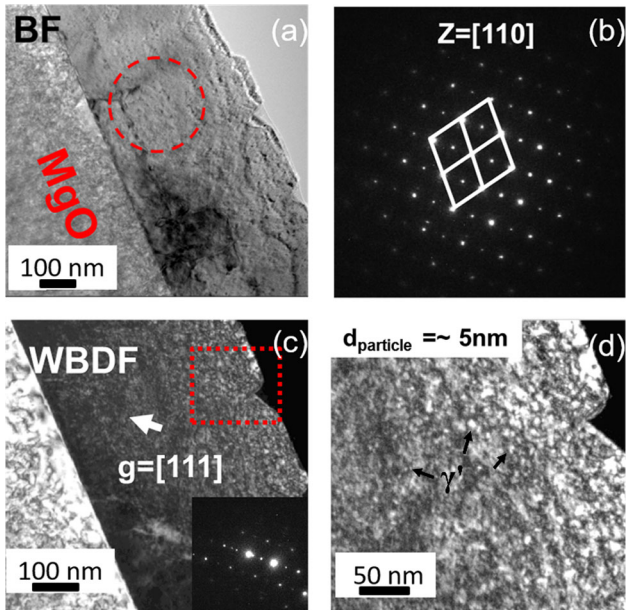

Fig. 3. Thermal stability of Ni/Ni_3Al multilayer under isothermal annealing at 1073 K for 1 h. (a) Bright-field (BF) TEM image of Ni/Ni_3Al after annealing. The Ni/Ni_3Al became discrete with precipitates forming on the interface. (b) SAD pattern of the region in the circle in (a) along zone axis [110]. The superlattice reflections confirm the presence of $L1_2$-ordered phase within the multilayer. (c) WBDF TEM micrograph with diffraction vector of $\mathbf{g} = [111]$. (d) Magnified micrograph of rectangular area in (c). A high density of γ' pherical particles with average diameter ($d_{particle}$) of $\sim$ 5 nm formed in the matrix.

schematic in Fig. 5b. The regions of irradiation and CHT were marked and separated for post-irradiation examination. Figure 6 shows the irradiated microstructure of Ni/Ni_3Al multilayer. Voids and dislocation loops were clearly observed within the film. Some faceted voids with size as large as 30 nm formed in the Ni–Al layer and Ni_3Al/Ni–Al interfaces. Void swelling was reported in pure Ni with 2–3% cold work after neutron irradiation (9–17 dpa) at elevated temperatures ranging from 673 to 823 K.[25] Dendritic voids were reported in Ni ion-irradiated Ni at 873 K to 20 dpa or at 923 K to 12 dpa.[26] In our study, no voids were observed in the Ni layer or Ni_3Al layer due to the relatively lower dose compared with the literature report, while voids formed in the Ni–Al layer. In the γ Ni–Al solid solution, Al diffusion is faster than Ni diffusion.[27] The addition of a relatively fast-diffusing element in Ni could result in an increase in the effective diffusivity of vacancies with an accompanying decrease in the irradiation-induced vacancy concentration, and thus could mitigate the void nucleation and growth. Experiments in literature also show that addition of Al up to 8 at.% in Ni can significantly decrease the swelling rate.[28,29] In our study, the formation of the voids in the Ni–Al layer is most likely caused by the defect imbalance effect near the free surface of the specimen. The defect imbalance phenomenon during ion irradiation has been described by Shao et al.[30]

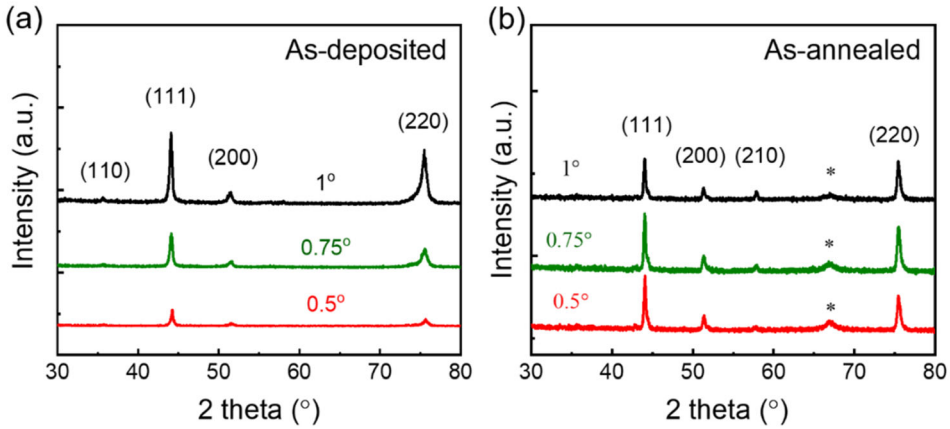

Fig. 4. GIXRD measurements of depth-dependent phase components in Ni/Ni_3Al multilayer with angles of incidence of 0.5°, 0.75°, and 1°: (a) as-deposited multilayer, and (b) as-annealed multilayer.

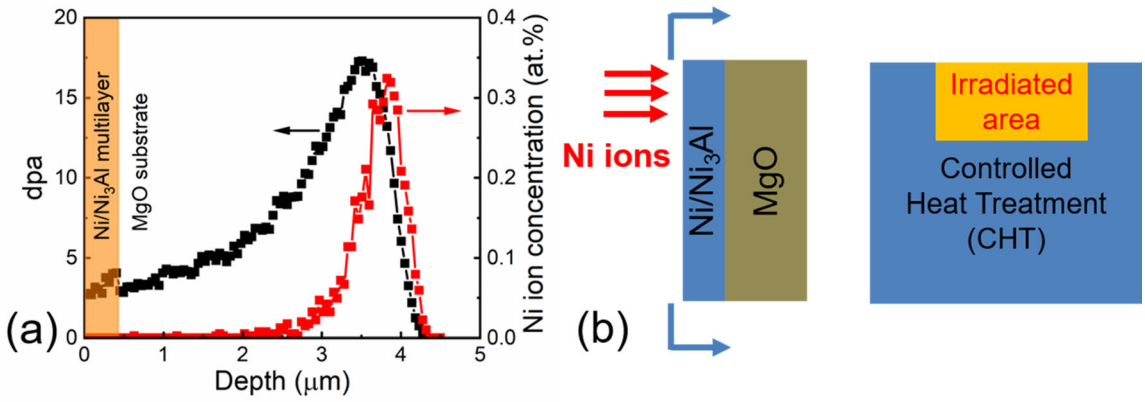

Fig. 5. (a) SRIM prediction of displacement damage and Ni ion concentration profiles in Ni/Ni_3Al multilayer under irradiation. The average displacement damage is ~ 3.5 dpa in the multilayer, with negligible injected Ni interstitials. (b) Schematic illustration of irradiation experiment setup. The controlled heat treatment area in the specimen underwent the same temperature condition as the irradiated area.

Figure 7 shows the evolution of the $L1_2$-ordered Ni_3Al phase under irradiation. SAD patterns of the as-deposited, CHT, and irradiated specimens were taken along the [001] zone axis. The superlattice reflections from $L1_2$-ordered Ni_3Al phase were present in the SAD patterns of the as-deposited, CHT, and irradiated specimens. The superlattice reflections of γ' (110) are labeled in the SAD patterns. Disordering and recovery are two competing processes in intermetallic compounds under irradiation. At low temperatures, irradiation-induced point defects, defect clusters, and antisite defects disrupt the ordered sites and induce disordering. The irradiation dose required to disorder γ' precipitates in Rene N4 is as low as 0.3 dpa at room temperature.[17] At elevated temperatures, the recovery process of disordered Ni_3Al is promoted due to the enhanced mobility of nonequilibrium vacancies,[31] thus to create a given degree of disorder, a higher irradiation fluence is required with increasing irradiation temperature. Figure 8 shows the chemical distribution profiles within the CHT and irradiated multilayers. EDS line scans were performed across the multilayer, including the MgO substrate and Ni, Ni_3Al, and Ni–Al layers. The vertical solid lines indicate the original location of the interfaces. In Fig. 8a, the Ni/Ni_3Al interface in the CHT specimen remained stable without significant chemical redistribution, while chemical intermixing occurred in the irradiated Ni/Ni_3Al interface, as seen in Fig. 8b. The width of the Ni/Ni_3Al interface increased from ~ 10 to ~ 60 nm after irradiation. Experimental studies[17, 29, 32] have reported that γ' precipitates disorder at a low dose (< 0.3 dpa) then gradually dissolve into the matrix at higher doses at room temperature. The dissolution of the γ' precipitates into the matrix is mainly caused by the thermal spike effect during irradiation at low temperatures. At higher temperatures, the disordered atoms tend to return to the equilibrium sites and reorder, which could postpone the dissolution process. It was noted that the Ni_3Al phase retained its ordered $L1_2$ structure after irradiation at 773 K, while chemical intermixing occurred at the interface between Ni and Ni_3Al.

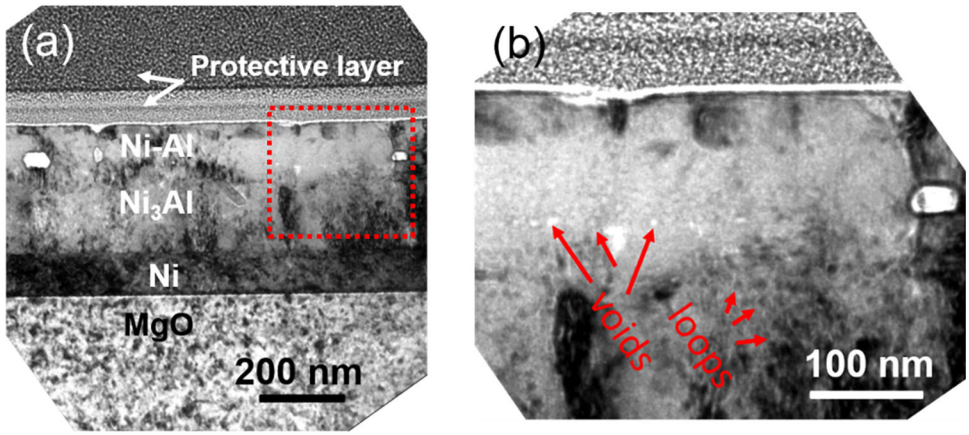

Fig. 6. TEM characterization of irradiated Ni/Ni_3Al multilayer. (a) Bright-field TEM micrograph, showing the formation of large voids in the Ni–Al top layer. (b) Magnified TEM micrograph of the area marked in (a). Large facet voids and small spherical voids formed near the surface region. Dislocation loops formed in the irradiated Ni and Ni_3Al layers.

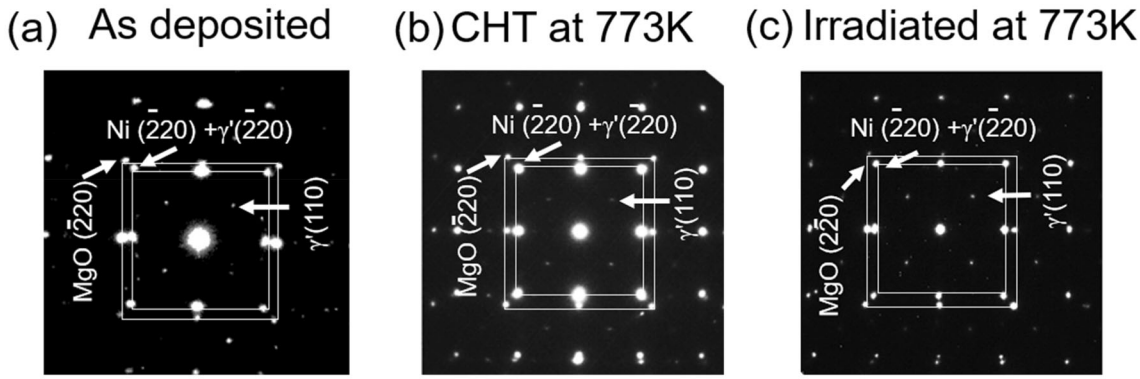

Fig. 7. Comparison of SAD patterns of Ni/Ni_3Al multilayer along [001] zone axis under different conditions, where the diffraction spots originate from γ' Ni_3Al, Ni, and MgO substrate: (a) as-deposited multilayer, (b) CHT multilayer, and (c) irradiated multilayer.

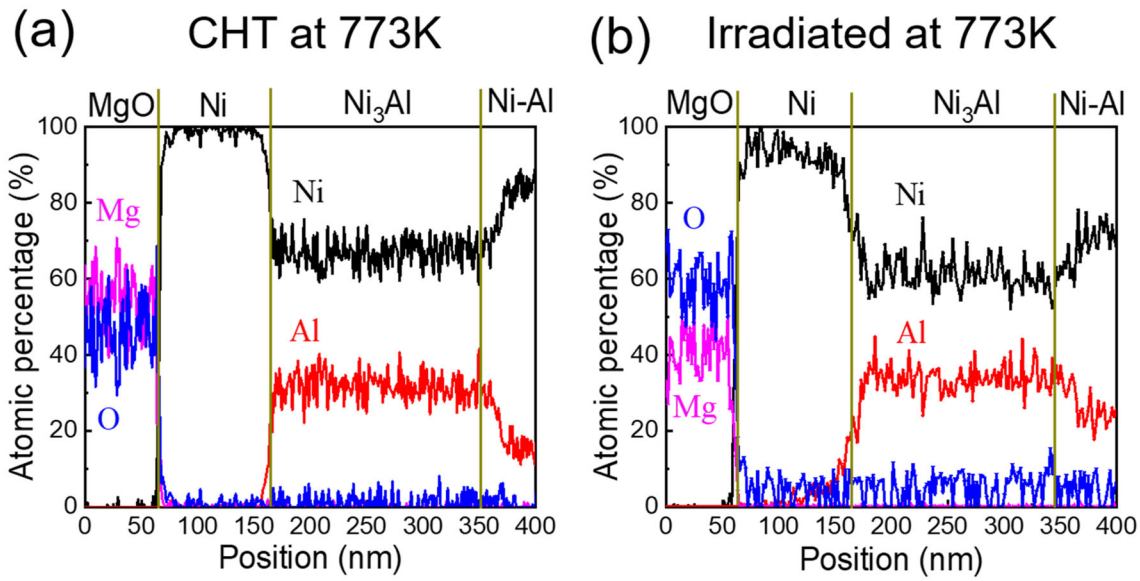

Fig. 8. Chemical distribution profiles of Ni/Ni_3Al multilayer: (a) CHT multilayer, and (b) Irradiated multilayer.

CONCLUSIONS

We studied the stability of Ni/Ni_3Al multilayer under thermal annealing and irradiation. The $L1_2$-ordered γ' Ni_3Al phase formed in the Ni/Ni_3Al multilayer when using magnetron sputtering at 773 K. When the layer thickness was less than 50 nm, the Ni/Ni_3Al interface became unstable due to chemical interdiffusion during sputtering at elevated temperature. After thermal annealing at 1073 K for 1 h, the Ni/Ni_3Al interface became discontinuous due to thermally induced interdiffusion and preferential precipitation on the interface. Under Ni ion irradiation to $\sim$ 3.5 dpa at 773 K, the formation of voids in the γ Ni–Al layer could result from the defect imbalance effect near the surface of the specimen. Irradiation-induced chemical intermixing occurred on the Ni/Ni_3Al interface, although the Ni_3Al phase retained its $L1_2$-ordered structure.

ACKNOWLEDGMENTS

We acknowledge support from the US Department of Energy (DOE) through the Los Alamos National Laboratory's Laboratory Directed Research & Development (LDRD) Program. Los Alamos National Laboratory, an affirmative action equal opportunity employer, is managed by Triad National Security, LLC for the US Department of Energy's NNSA, under Contract 89233218CNA000001. This work was also supported by the Idaho National Laboratory's LDRD Program under the US DOE Idaho operations office under Contract DE-AC07-051D14517. We also acknowledge the US DOE, Office of Nuclear Energy Nuclear Science User Facility under Contract DE-AC07-051D14517 and Office of Sciences User Facility Center for Integrated Nanotechnologies at Los Alamos National Laboratory under Contract 89233218CNA000001.

REFERENCES

1. S. Mori, H. Miura, S. Yamazaki, T. Suzuki, Y. Seki, T. Kunugi, S. Nishio, N. Fujisawa, A. Hishinuma, and M. Kikuchi, *Fusion Technol.* 21, 1744 (1992).
2. K. Nakata, K. Fukai, A. Hishinuma, K. Ameyama, and M. Tokiazane, *J. Nucl. Mater.* 202, 39 (1993).
3. W.J.S. Yang, *J. Nucl. Mater.* 108–109, 339 (1982).
4. Q. Gao, R.Y. Liu, J.S. Zhang, and J.T. Guo, *Mater. Lett.* 59, 2052 (2005).
5. W. Ren and R. Swimdeman, *J. Press. Vessel Technol.* 131(2), 024002 (2008). https://doi.org/10.1115/1.2967885.
6. X.H. Yu, Y. Yamabe-Mitarai, and H. Harada, *Scr. Mater.* 43, 671 (2000).
7. X.K. Meng, H. Shen, H. Vehoff, S. Mathur, and A.H.W. Ngan, *J. Mater. Res.* 17, 790 (2002).
8. X. Yang, X. Peng, and F. Wang, *Scr. Mater.* 56, 509 (2007).
9. S.J. Zinkle and G.S. Was, *Acta Mater.* 61, 735 (2013).
10. A.M. Ges, O. Fornaro, and H.A. Palacio, *Mater. Sci. Eng. A* 458, 96 (2007).
11. X. Xia, Y. Peng, J. Zhang, X. He, S. Yin, J. Ding, C. Li, X. Chen, and Y. Liu, *J. Mater. Sci.* 54, 13368 (2019).
12. H.M. Tawancy, *Metall. Microst. Anal.* 6, 200 (2017).
13. A.J. Ardell, *High Temperature Aluminides and Intermetallics*, ed. S.H. Whang, D.P. Pope, and C.T. Liu (Elsevier, Amsterdam, 1992), p. 212.
14. H.C. Liu and T.E. Mitchell, *Acta Metall.* 31, 863 (1983).
15. B. Sencer, G. Bond, F. Garner, M. Hamilton, S. Maloy, and W. Sommer, *J. Nucl. Mater.* 296, 145 (2001).
16. T.M. Angeliu, J.T. Ward, and J.K. Witter, *J. Nucl. Mater.* 366, 223 (2007).
17. C. Sun, M. Kirk, M. Li, K. Hattar, Y. Wang, O. Anderoglu, J. Valdez, B.P. Uberuaga, R. Dickerson, and S.A. Maloy, *Acta Mater.* 95, 357 (2015).
18. B.H. Sencer, G.M. Bond, F.A. Garner, M.L. Hamilton, B.M. Oliver, L.E. Thomas, S.A. Maloy, W.F. Sommer, M.R. James, and P.D. Ferguson, *J. Nucl. Mater.* 283–287, 324 (2000).
19. M.J. Sabochick and N.Q. Lam, *Phys. Rev. B* 43, 5243 (1991).
20. C. Zhang, K. Feng, Z. Li, F. Lu, J. Huang, and Y. Wu, *Appl. Surf. Sci.* 378, 408 (2016).
21. R. Banerjee, G.B. Thompson, P.M. Anderson, and H.L. Fraser, *Thin Solid Films* 424, 93 (2003).
22. A.L. Greer and H. Assadi, *Mater. Sci. Eng. A* 226–228, 133 (1997).
23. C. Sun, E. Martínez, J.A. Aguiar, A. Caro, J.A. Valdez, K. Baldwin, Y. Xu, B.P. Uberuaga, O. Anderoglu, and S.A. Maloy, *Mater. Res. Lett.* 3, 169 (2015).
24. P.Y. Li, H.M. Lu, S.C. Tang, and X.K. Meng, *J. Alloys Compd.* 478, 240 (2009).
25. S.I. Porollo, A.M. Dvoriashin, Y.V. Konobeev, and F.A. Garner, *J. Nucl. Mater.* 442, 809 (2013).
26. L. Chen and A. Ardell, *Scr. Metall.* 11, 871 (1977).
27. M. Watanabe, Z. Horita, D.J. Smith, M.R. McCartney, T. Sano, and M. Nemoto, *Acta Metall. Mater.* 42, 3381 (1994).
28. R. Pinizzotto, L. Chen, and A. Ardell, *Metall. Trans. A* 9, 1715 (1978).
29. E. Camus, C. Abromeit, F. Bourdeau, N. Wanderka, and H. Wollenberger, *Phys. Rev. B* 54, 3142 (1996).
30. L. Shao, C.C. Wei, J. Gigax, A. Aitkaliyeva, D. Chen, B.H. Sencer, and F.A. Garner, *J. Nucl. Mater.* 453, 176 (2014).
31. J. Ewert and G. Schmitz, *Eur. Phys. J. B Condens. Matter Complex Syst.* 17, 391 (2000).
32. T. Lee, A. Caro, and M.J. Demkowicz, *J. Mater. Res.* 30, 1456 (2015).